Article:
Brown, N.D. and Rhodes, E.J. orcid.org/0000-0002-0361-8637 (2019) Dose-rate dependence of natural TL signals from feldspars extracted from bedrock samples. Radiation Measurements. ISSN 1350-4487

https://doi.org/10.1016/j.radmeas.2019.106188

Dose-rate dependence of natural TL signals from feldspars extracted from bedrock samples

N.D. Brown[a,b,*], E.J. Rhodes[c]

[a]*Department of Earth and Planetary Sciences, University of California, Berkeley, CA, USA*
[b]*Berkeley Geochronology Center, 2455 Ridge Road, Berkeley, CA, USA*
[c]*Department of Geography, Winter Street, University of Sheffield, Sheffield, South Yorkshire S10 2TN, UK*

Published in Radiation Measurements, https://doi.org/10.1016/j.radmeas.2019.106188 Author accepted version

Abstract

The influence of dose rate on feldspar thermoluminescence shape is considered for a variety of natural dose rates. The geologic dose rate experienced by bedrock samples is observed to control the position of the low-temperature edge of the bulk TL signal (the $T_{1/2}$ parameter), with higher dose rates producing natural TL signals that begin to emit at lower measurement temperatures. This behavior can be explained in terms of the natural equilibrium between electron trapping and detrapping rates, as the trapping rate depends directly on the dose rate. The role of anomalous fading is more subtle. While a wide range of $T_{1/2}$ values is found at low fading rates, only high $T_{1/2}$ values are found when the fading rate is greater. This suggests that high fading rates may also influence the natural $T_{1/2}$ value by making low-temperature regions of the TL curve unstable. Our results illustrate the need to consider dose-rate and fading-rate variations between bedrock samples before interpreting the minimum stability of each natural TL signal, a consequential result for future low-temperature thermochronology applications.

Keywords: geologic dose rate, feldspar thermoluminescence, low-temperature thermochronology, anomalous fading

1. Introduction

Whether a set of traps accumulate or lose electrons through time depends on the balance between the rate of free electrons produced by ionizing radiation, i.e., the dose rate, $\dot{D}$, and the average probability per unit time of detrapping, p, which is the inverse of the trap lifetime, τ. This has an interesting consequence. Imagine that all traps in a crystal were emptied and then subjected to geologic burial. After some time there would exist some trap types that were in 'field saturation' or

*Corresponding author
Email addresses: nathan.brown@berkeley.edu (N.D. Brown), ed.rhodes@sheffield.ac.uk (E.J. Rhodes)

steady state, meaning that the rate of trapping at geologic conditions is the same as the loss rate (Huntley and Lian, 2006; Kars et al., 2008). Other traps will still be experiencing net accumulation. If this crystal were analyzed and the equivalent doses (D_e) were determined for all trap types, the D_e values for accumulating traps would indicate the time since traps were empty and the D_e values for the static traps would represent the average trap lifetime, as illustrated by the following equation (Grün et al., 1999):

$$D_e = \dot{D} \cdot \tau \left[1 - \exp(-t/\tau) \right] \tag{1}$$

This principle is the basis for 'age-plateau' analysis commonly used in TL dating (e.g., p. 64, Fleming, 1979).

According to Eq. 1, the magnitude of the dose rate and the rate of detrapping (a function of ambient temperature) control the degree to which sites will be filled (Christodoulides et al., 1971; Ypma and Hochman, 1991). The degree of site saturation, usually expressed as n/N, is the target measurement in most luminescence thermochronology research (for a recent review, see King et al., 2016a), but most of the experimental research to date has considered variations in laboratory or natural thermal conditions while variations in dose rates have been restricted to a narrow range (e.g., factor 1.6 difference in beta dose rates and the resulting infrared stimulated luminescence signal; Guralnik et al., 2015).

The aim of this study is to measure how TL signals from bedrock feldspars vary following a wide range of natural dose rates. As feldspars extracted from bedrock samples have been explored for use in low-temperature thermochronometry (Brown et al., 2017; Tang and Li, 2017; Biswas et al., 2018), we examine how surficial bedrock samples from the same glacial valley yield natural TL signals which vary in shape as a linear function of geologic dose rate. By comparison, measured fading values do not correlate strongly with the position of the leading edge of emissions. Our results are discussed in light of future thermochronology efforts involving samples with different geologic dose rates.

2. How geologic dose rate relates to the natural TL shape

To understand how the dose rate $\dot{D}$ is expected to affect electron trap site stability, we consider the electron trapping rate equation from Brown et al. (2017):

$$\frac{dn(r')}{dt} = \frac{\dot{D}}{D_0}\Big(N(r') - n(r') \Big) - n(r') \exp\Big(-\Delta E/k_B T \Big) \frac{P(r')s}{P(r') + s} \tag{2}$$

where $n(r')$ and $N(r')$ are the concentrations (m^{-3}) of occupied and total traps, respectively, at some recombination distance r'; D_0 is the characteristic dose of saturation (Gy); ΔE is the activation energy (eV) required for thermally-activated tunneling; T is the sample temperature (K); k_B is the Boltzmann constant; $P(r')$ is the tunneling probability at some distance r' (s^{-1}); and s is the frequency factor (s^{-1}). We can see that the distance r' between the electron trap and the nearest recombination center influences site stability; nearer sites are more likely to recombine and will therefore have a shorter mean lifetime (Huntley, 2006). This effect is enhanced at higher temperatures as more electrons are excited to higher-energy states where tunneling becomes more probable (Jain et al., 2012, 2015). This temperature dependence is the underlying principle for feldspar TL thermochronology (Pagonis and Brown, 2019).

Assuming that all of the blue emissions from feldspar natural TL between measurement temperatures of about 130 - 330 °C are from the same defect (Krbetschek et al., 1997) – below the $\sim$ 410 °C TL peak identified by Murray et al. (2009) as the main dosimetric trap for the IRSL signal – and assuming that the only difference between the TL measured in that temperature range is the stability of those detrapping sites, we can approximately describe the thermal stability of the bulk TL emissions by the position of the $T_{1/2}$ metric (Fig. 1). Because the TL measurement temperature at which emissions become significant is a function of the occupied sites of minimum stability, and because the $T_{1/2}$ value is a convenient and (usually) unambiguous measurement, we treat measured $T_{1/2}$ values as representing the characteristic (minimum) thermal stability of the feldspar bulk TL signal (Spencer and Sanderson, 1994, 2012; Chen and Pagonis, 2011, Ch. 5).

In the case of widely varying steady-state temperatures, $T_{1/2}$ values are shown to largely be a function of long-term rock temperature (Brown et al., 2017). If, however, several bedrock samples have been held at a similar temperature, their natural $T_{1/2}$ values may reflect higher-order influences like dose-rate variations or differences in fading rates.

The bedrock samples collected from Rock Creek glacial valley lend themselves to this analysis. Collected from within a single valley and all from near the ground surface, these samples experienced similar mean annual air temperature since their exposure: instrumental temperature records combined with the dry adiabatic lapse rate should result in mean annual temperatures ranging from about -7.0 to 1.0 °C between the highest- and lowest-elevation samples considered in this section. The valley-bottom temperature is based on the mean annual temperatures recorded between 1892 and 2012 in the nearby town of Red Lodge, MT (elevation 1697 masl), which are freely available from the Western Regional Climate Center website: www.wrcc.dri.edu. Furthermore, the geologic

dose rates for these samples vary by a factor of 9.7 (Table 1), an unusually high difference.

While the focus of this study is the dose-rate dependence of natural $T_{1/2}$ values, we also consider whether a sample's fading rate is a good predictor of $T_{1/2}$. As will be shown with fading measurements in Section 5.2, though fading is not strongly correlated to $T_{1/2}$, it may still limit the stability of the bulk TL signal in feldspars.

3. Sample collection, preparation, and measurement details

The feldspar samples measured in this study were taken from the tectonically uplifted crustal block known as the Beartooth uplift, located near the town of Red Lodge, Montana, USA. This uplifted region is a 60 × 125 km block of Precambrian crystalline basement which was initially exhumed during the Laramide orogeny, a period of mountain building in the western USA between ∼80 to 35 Mya (Wise, 2000). Apatite fission-track results from a 2.5-km-deep exploratory well indicate a two-stage uplift history, with the first stage beginning around 61 Ma and resulting in 4 - 8 km of uplift, and the second stage beginning between 15 and 5 Ma and producing about 4 km of uplift, which continues to the present (i.e., 0.3 - 0.8 mm/yr) (Omar et al., 1994).

Bedrock samples were detached by sledge hammer and chisel from rock outcrops that seemed to be in place (i.e., not 'float'). The latitude, longitude, and elevations of sample collection locations were measured with a handheld GPS system. After sample collection, the bedrock samples were spray-painted with a contrasting color and then broken into smaller pieces under dim amber LED lighting in the laboratory. The sunlight-exposed, outer-surface portions of the samples were separated from the inner portions.

The unexposed inner portions from the samples were then crushed by hand using a pestle and mortar and sieved to isolate the 175 - 400 μm size fraction. These separates were then treated with 3% hydrochloric acid and separated by density using lithium metatungstate heavy liquid ($\rho < 2.565$ g/cm^3; Rhodes 2015) in order to isolate the most potassic feldspar grains. Grains were mounted on stainless steel discs in a small-diameter (3 - 5 mm) monolayer using silicon oil. No hydrofluoric acid was used to etch these crystals.

All luminescence measurements were performed at the UCLA luminescence laboratory using a TL-DA-20 Risø automated reader equipped with a ^{90}Sr/^{90}Y beta source which delivers 0.1 Gy/s at the sample location (Bøtter-Jensen et al., 2003). Emissions were detected through a Schott BG3-BG39 filter combination (transmitting between ∼325 - 475 nm), thermoluminescence measurements were performed in a nitrogen atmosphere and glow curves were measured at a heating rate of 5 °C/s.

Table 1: Dosimetry information. See Section 4 for details.

Sample	Lat. (°N)	Long. (°W)	Elev. (masl)	K (wt.%)	Th (ppm)	U (ppm)	Grain size (μm)	Internal K (wt.%)	Total dose rate (Gy/ka)
J0994	45.038	109.408	2940	7.0	4.5	0.57	237 ± 141	13.8 ± 0.13[a]	8.78 ± 0.72
J0995	45.038	109.409	2895	0.7	11.8	0.76	225 ± 137	0.04 ± 0.02	2.36 ± 0.14
J0996	45.041	109.409	2781	2.3	2.2	1.34	39 ± 20	12.5 ± 0.5[b]	3.85 ± 0.17
J0997	45.042	109.409	2735	2.2	2.4	1.53	41 ± 22	12.5 ± 0.5[b]	3.84 ± 0.17
J1000	45.044	109.414	2518	1.5	13.2	0.70	275 ± 178	12.5 ± 0.5[b]	4.16 ± 0.69
J1001	45.048	109.417	2315	2.1	2.3	0.69	231 ± 139	13.9 ± 0.06	3.79 ± 0.60
J1002	45.050	109.423	2241	2.4	18.7	2.54	261 ± 156	13.8 ± 0.13[a]	5.98 ± 0.69
J1003	45.038	109.440	2856	0.6	1.0	0.32	277 ± 164	13.8 ± 0.13[a]	2.34 ± 0.69
J1004	45.043	109.439	2691	0.2	2.3	0.25	287 ± 166	0.04 ± 0.02[c]	0.90 ± 0.05
J1006	45.050	109.432	2449	2.2	1.5	1.63	41 ± 21	12.5 ± 0.5[b]	3.75 ± 0.17
J1007	45.003	109.517	2636	3.6	26.9	3.40	254 ± 140	13.8 ± 0.13[a]	8.03 ± 0.67
J1010	45.076	109.381	2131	2.4	9.4	1.27	281 ± 176	13.8 ± 0.13[a]	4.95 ± 0.76

[a]Average value of separated material from granitic samples J0999 and J1001.

[b]Huntley and Baril (1997).

[c]Measured value from J0995, a tonalite like J1004.

The thermal background was measured and then subtracted from each glow curve.

4. Geologic dose rate determination

The outer portions of each bedrock sample were analyzed by inductively-coupled plasma mass spectrometry (ICP-MS) to estimate the U and Th contents, and with inductively-coupled optical emission spectrometry (ICP-OES) to measure the K content. The alpha and beta dose-rates were calculated using the conversion factors of Liritzis et al. (2013), the alpha and beta attenuation factors of Brennan et al. (1991) and Guérin et al. (2012), respectively, and an a-value of 0.15 ± 0.05, as recommended for coarse-grained K-feldspars (Balescu and Lamothe, 1994). Beta attenuation is calculated assuming a water content of 1 ± 1%. The original feldspar grain sizes were estimated following the approach of King et al. (2016b), who processed images of petrographic thin sections using the grain size analysis software of Buscombe (2013) (see the Supplementary Materials for the

detailed results).

The internal potassium values were estimated as follows. Three samples from this site were analyzed with electron microprobe analysis in a previous study (Brown and Rhodes, 2017): J0995, J0999, and J1001. Because J0999 and J1001 are granitic gneisses, the other granitic gneiss samples (J0994, J1002, J1007 and J1010) and granitoid gneiss (J1003) were given the mean value of the two samples: 13.8 ± 0.13 wt.%. Sample J1004 shares the value of J0995 (0.04 ± 0.02 wt.%) because both are tonalitic gneisses. The remaining samples, three dacite porphyries (J0996, J0997, and J1006) and one granodiorite gneiss (J1000) were assigned the conservative value from Huntley and Baril (1997) of 12.5 ± 0.5 wt.%.

Cosmic dose rates were estimated using the geomagnetic latitude along with a shielding depth. A shielding depth of 5 ± 5 cm was used, as this represents the typical radius of collected specimens (a shielding density of 2.65 g/cm^3 was used). The geologic dose rate was calculated using the DRAC software package, v1.2 (Durcan et al., 2015), and the resulting values are listed in Table 1.

5. Results

5.1. Relationship between $T_{1/2}$ and geologic dose rate

The natural $T_{1/2}$ values measured at a heating rate of 5 °C/s are plotted as a function of geologic dose rate ($\dot{D}$) in Fig. 2. The sizes of the error bars are determined by the between-aliquot variation, as TL curves were measured from three discs for most samples (only two discs were measured for samples J1007 and J1010). Samples J0999, J1008, and J1009 were excluded from this analysis, as the location of $T_{1/2}$ was ambiguous (see Supplementary Materials). A linear relationship is found, and as expected, as $\dot{D}$ increases the natural TL curves exhibit lower $T_{1/2}$ values. The interpretation is that these less stable sites (lower $T_{1/2}$ values) remain occupied because there are more free electrons roaming the lattice at any given moment due to the greater flux of ionizing radiation.

The best-fit line for the dependence of $T_{1/2}$ on $\dot{D}$ is given as

$$T_{1/2} = (-2.38 \pm 0.50)\dot{D} + (242.3 \pm 2.6). \quad (3)$$

This regression was performed using the updated York fitting, appropriate for data with multivariate errors (Mahon, 1996), and the mean square weighted deviate (MSWD) value of 0.90 suggests a robust linear relationship. The slope of this line, -2.38 ± 0.50 °C Gy^{-1} ka^{-2} is particularly noteworthy, suggesting the magnitude of this dose-rate dependence. As a side note, the range in dose rates observed for these samples is probably close to the natural variation expected for bedrock feldspars,

Table 2: Sample characteristics.

Sample	Lithology	$\rho' \times 10^4$	$T_{1/2}$ (°C)	Dose rate (Gy/ka)
J0994	Granitic gneiss	10.9 ± 4.9	227.7 ± 6.4	8.78 ± 0.72
J0995	Tonalitic gneiss	7.3 ± 4.8	241.2 ± 11.8	2.36 ± 0.14
J0996	Dacite porphyry	1.8 ± 0.7	231.7 ± 2.2	3.84 ± 0.19
J0997	Dacite porphyry	2.7 ± 1.9	236.4 ± 4.5	3.83 ± 0.21
J1000	Granodiorite gneiss	2.7[a]	235.5 ± 4.5	4.16 ± 0.69
J1001	Granitic gneiss	2.1[a]	223.2 ± 6.9	3.79 ± 0.60
J1002	Granitic gneiss	3.3[a]	232.2 ± 5.2	5.98 ± 0.69
J1003	Granitoid gneiss	22.5 ± 11.8	239.0 ± 5.8	2.34 ± 0.69
J1004	Tonalitic gneiss	31.7 ± 16.5	236.6 ± 3.5	0.90 ± 0.05
J1006	Dacite porphyry	4.5[a]	238.5 ± 6.0	3.73 ± 0.20
J1007	Granitic gneiss	3.9 ± 1.5	220.3 ± 2.2	8.03 ± 0.67
J1010	Granitic gneiss	2.0 ± 0.7	233.1 ± 1.9	4.95 ± 0.76

[a]One of two discs omitted.

so this plot may prove useful in quantifying the maximum dependence of $T_{1/2}$ on dose rate for a suite of samples.

5.2. Relationship between $T_{1/2}$ and room-temperature fading

So far, we have considered the variation in geologic dose rate and how the resulting change in the trap filling rate controls the minimum stability (i.e., $T_{1/2}$ position) of the bulk TL signal. In this section, we will consider a competing effect: the degree to which trap emptying by room-temperature fading may control the $T_{1/2}$ position.

To quantify this effect, samples were given a beta dose of 5.1 Gy and then kept a room temperature for a period of time before measurement. Two aliquots per sample were each measured following nine pauses of different lengths. The shortest pause for every sample was 54 s and the longest pause ranged from 15.5 to 19.8 d. These delayed TL measurements, as well as their respective $T_{1/2}$ values plotted as a function of delay time, are provided in the Supplementary Materials.

Generally, samples exhibit a logarithmic increase in $T_{1/2}$ as a function of delay time, though some samples exhibited more complicated behavior (see Supplementary Materials for the entire dataset). Fig. 3 illustrates the behavior exhibited by samples J0995, J1003, and J1004. Notice the kink in

the plot of $T_{1/2}$ versus effective fading time for sample J1003 (inset of Fig. 3a) as contrasted with sample J1007, which shows logarithmic growth in $T_{1/2}$ over the entire range of fading times. This difference in behavior seems to stem from the prominent peak centered at about 103 °C (Fig. 3a). This peak decays at room temperature with a half-life of about 1.7 hrs. The position and lifetime of this peak are similar to the 110°C TL peak in quartz (Schmidt et al., 2018) and may indicate some contamination of the signal by quartz. After this peak decays by about two half-lives, or about 1.2×10^4 s, the $T_{1/2}$ of this sample increases logarithmically with time at a similar rate to J1007 (Fig. 3b).

Samples J0994, J0996, J0997, and J1000 showed a logarithmic increase in $T_{1/2}$, but at delay times greater than $\sim 10^5$ s, $T_{1/2}$ values were offset to lower temperatures, despite a similar rate of growth (see Supplementary Materials). This behavior is related to a loss of TL centered at ~ 180 °C and extending up to ~ 300 °C, though the reason for this loss is unclear. Because of the irregular behavior at shorter durations and because all samples exhibited logarithmic increases in $T_{1/2}$ with delay times $>\sim 10^5$ s, we consider only those longest three delay points for each aliquot in the following analysis.

The $T_{1/2}$ fading data were used to constrain the ρ' values of these samples (Huntley, 2006), assuming that tunneling proceeds via the excited state (Jain et al., 2012, 2015). Note that for a given fading dataset, this assumption will produce higher best-fit ρ' values than if ground-state tunneling were assumed (cf. Biswas et al., 2018). Best-fit ρ' values were determined by simulating irradiation and fading at room temperature ($T = 18$°C) with Eq. 2. The $n(r')$ array for each sample allowed to evolve through time with an ordinary differential equation solver in MATLAB; see Brown et al. (2017) for more details on this approach. We used the following parameter values: the attempt-to-tunnel frequency factor $P_0 = 4.6 \times 10^{14}$ s^{-1} (p. 168; Brown, 2017); the attempt-to-escape frequency factor $s = 4.2 \times 10^{12}$ s^{-1} (the Debye frequency of K-feldspar; Anderson and Liebermann, 1966; Anderson, 1995); and the characteristic dose $D_0 = 1.6$ kGy (Brown et al., 2017). Three variables were solved for by minimizing the misfit between observed and simulated $T_{1/2}$ values: the thermal depth of the excited state E_e was allowed to vary between 0.75 and 1.20 eV; the ground state depth E_g could vary betweeen 1.70 and 2.15 eV, and ρ could vary between 5×10^{25} and 5×10^{27} m^{-3}, which translates to a ρ' value of 4.2×10^{-2} and 2.1×10^{-4} for $E_e = 1.1$ eV. Following optimization to find the best-fit ρ' value for each sample (Table 2), the simulated $T_{1/2}$ values closely match observations of room temperature fading on timescales of days to weeks, with an average coefficient of determination of $R^2 = 0.90 \pm 0.12$ (see Supplementary Materials for all

results).

This approach also reproduces the form of fading within individual glow curve temperature ranges, as shown in Fig. 4. The observations in Fig. 4b come from sample J0165, a bedrock-extracted K-feldspar sample examined in detail within Brown and Rhodes (2017). The model parameters in panel b represent typical values for our samples. This figure illustrates how Eq. 2 generally replicates the decay form of regenerative TL curves during room temperature storage. At lower glow curve temperatures, the decay is not logarithmic but has a decreasing slope when plotted on a semi-log plot. Moving to higher glow curve temperatures, the curves resemble inverted sigmoids and eventually flat lines (i.e., no decay). Notice that at some bins, these data could be approximately fitted to distinct g-values, but we favor our approach of fitting the fading TL curves to a single ρ' value as being more parsimonious and physically meaningful (Kars et al., 2008). This can be contrasted with the approach of Biswas et al. (2018), who divided their feldspar TL glow curves into discrete temperature bin ranges and independently fitted data within each range to the kinetic expression of Guralnik et al. (2015). The approach of Biswas et al. (2018) implies that the feldspar TL curve represents not a continuum of stability arising from different tunneling distances (as we assume here), but instead a series of unrelated traps, each governed by individual kinetic parameters (see also Sanderson, 1988; Pagonis et al., 2014).

The motivating question for this section is the degree to which fading rates control $T_{1/2}$ values. To address this question, we plot the $T_{1/2}$ and ρ' values for every aliquot in Fig. 5. We make two observations about these results. The first is the lack of correlation between the variables. For comparison with Fig. 2, we perform a linear regression. The MSWD value for this regression, 3.47, is well outside the 95% confidence interval range: $0.457 - 1.750$ (Mahon, 1996), which implies a bad fit. The second observation is that the variance of the $T_{1/2}$ values decreases with higher ρ' values, such that at high ρ' values only high values of $T_{1/2}$ exist. One possible interpretation is that at higher ρ' values, room-temperature fading may place a limit on the stability of the natural TL curve. In other words, while much of the variation found at lower ρ' values may be explained by other factors (e.g., geologic temperature or dose rate), at higher ρ' values the fading rate may prevent lower temperature regions of the TL curve from populating. This unstable region is illustrated in blue in Fig. 5.

6. Conclusions

Brown et al. (2017) recently showed that feldspar samples with similar geologic dose rates and

very different burial temperatures ($-4 - 60$°C) exhibit a linear relationship between the position of the TL leading edge, $T_{1/2}$, and geologic temperature. In the present study, we have presented feldspars from a glacial valley that have been at atmospheric temperatures for at least several thousand years, but that exhibit a wide range of geologic dose rates, from 0.9 to 8.8 Gy/ka. These samples show a linear relationship between $\dot{D}$ and $T_{1/2}$. The slope of the best-fit line, -2.38 $\pm$ 0.50 °C Gy^{-1} ka^{-2}, provides a first approximation at the magnitude of this effect, which should prove to be a useful correction when differentiating between thermal and non-thermal controls on natural TL shapes. The poor fit between ρ' and $T_{1/2}$ indicates that for these samples, the primary control on the minimum stability of TL is not fading. However, the lack of low $T_{1/2}$ values for samples with high ρ' values (i.e., the lack of natural TL populations at low-temperatures when fading is high) may indicate that fading can, nonetheless, prevent sites from accumulating in nature Valla et al. (2016), to the extent that the $T_{1/2}$ is affected. All of these effects are consistent with the kinetic model referenced at the beginning of this paper, where tunneling to the nearest neighbor is the primary loss pathway for trapped charge.

For future work in feldspar TL thermochronology, we recommend one of two approaches when collecting samples and interpreting results. By choosing a site with uniform lithology, and presumably similar fading rates and environmental dose rates, these effects might be minimized. Alternately, if differences in dose rate between samples are significant or if samples experience high fading rates, the position of the leading edge of emissions ($T_{1/2}$) may require correction (e.g., using the slope of the best-fit line to normalize $T_{1/2}$ values). In the case of high dose rates, $T_{1/2}$ values might be lower than for samples at the same temperature but with lower dose rates. In the case of high fading rates, the $T_{1/2}$ values might be higher than expected due to fading-induced instability in the low-temperature regions of the glow curve.

Acknowledgements

We would like to thank two anonymous reviewers for their insightful comments. NDB is supported by NSF award 1806629.

References

Anderson, O.L., 1995. Equations of state of solids for Geophysics and ceramic science. Oxford University Press.

Anderson, O.L., Liebermann, R.C., 1966. Sound velocities in rocks and minerals. Technical Report. Willow Run Laboratories, University of Michigan.

Balescu, S., Lamothe, M., 1994. Comparison of TL and IRSL age estimates of feldspar coarse grains from waterlain sediments. Quaternary Science Reviews 13, 437–444.

Biswas, R.H., Herman, F., King, G.E., Braun, J., 2018. Thermoluminescence of feldspar as a multi-thermochronometer to constrain the temporal variation of rock exhumation in the recent past. Earth and Planetary Science Letters 495, 56–68.

Bøtter-Jensen, L., Andersen, C.E., Duller, G.A.T., Murray, A.S., 2003. Developments in radiation, stimulation and observation facilities in luminescence measurements. Radiation Measurements 37, 535–541.

Brennan, B.J., Lyons, R.G., Phillips, S.W., 1991. Attenuation of alpha particle track dose for spherical grains. Nuclear Tracks and Radiation Measurements 18, 249–253.

Brown, N.D., 2017. Using luminescence signals from bedrock feldspars for low-temperature thermochronology. Ph.D. thesis. University of California, Los Angeles.

Brown, N.D., Rhodes, E.J., 2017. Thermoluminescence measurements of trap depth in alkali feldspars extracted from bedrock samples. Radiation Measurements 96, 53–61.

Brown, N.D., Rhodes, E.J., Harrison, T.M., 2017. Using thermoluminescence signals from feldspars for low-temperature thermochronology. Quaternary Geochronology 42, 31–41.

Buscombe, D., 2013. Transferable wavelet method for grain-size distribution from images of sediment surfaces and thin sections, and other natural granular patterns. Sedimentology 60, 1709–1732.

Chen, R., Pagonis, V., 2011. Thermally and optically stimulated luminescence: A simulation approach. Wiley.

Christodoulides, C., Ettinger, K.V., Fremlin, J.H., 1971. The use of TL glow peaks at equilibrium in the examination of the thermal and radiation history of minerals. Modern Geology 2, 275–280.

Durcan, J.A., King, G.E., Duller, G.A.T., 2015. DRAC: Dose Rate and Age Calculator for trapped charge dating. Quaternary Geochronology 28, 54–61.

Fleming, S., 1979. Thermoluminescence techniques in archaeology. Oxford University Press.

Grün, R., Tani, A., Gurbanov, A., Koschug, D., Williams, I., Braun, J., 1999. A new method for the estimation of cooling and denudation rates using paramagnetic centers in quartz: A case study on the Eldzhurtinskiy Granite, Caucasus. Journal of Geophysical Research 104, 17531–17549.

Guérin, G., Mercier, N., Nathan, R., Adamiec, G., Lefrais, Y., 2012. On the use of the infinite matrix assumption and associated concepts: A critical review. Radiation Measurements 47, 778–785.

Guralnik, B., Jain, M., Herman, F., Ankjaergaard, C., Murray, A.S., Valla, P.G., Preusser, F., King, G.E., Chen, R., Lowick, S.E., Kook, M., Rhodes, E.J., 2015. OSL-thermochronometry of feldspar from the KTB borehole, Germany. Earth and Planetary Science Letters 423, 232 – 243.

Huntley, D.J., 2006. An explanation of the power-law decay of luminescence. Journal of Physics: Condensed Matter 18, 1359–1365.

Huntley, D.J., Baril, M.R., 1997. The K content of the K-feldspars being measured in optical dating or in thermoluminescence dating. Ancient TL 15, 11–13.

Huntley, D.J., Lian, O.B., 2006. Some observations on tunnelling of trapped electrons in feldspars and their implications for optical dating. Quaternary Science Reviews 25, 2503–2512.

Jain, M., Guralnik, B., Andersen, M.T., 2012. Stimulated luminescence emission from localized recombination in randomly distributed defects. Journal of Physics: Condensed Matter 24, 385402.

Jain, M., Sohbati, R., Guralnik, B., Murray, A.S., Kook, M., Lapp, T., Prasad, A.K., Thomsen, K.J., Buylaert, J.P., 2015. Kinetics of infrared stimulated luminescence from feldspars. Radiation Measurements 81, 242–250.

Kars, R., Wallinga, J., Cohen, K., 2008. A new approach towards anomalous fading correction for feldspar IRSL dating–tests on samples in field saturation. Radiation Measurements 43, 786–790.

King, G.E., Guralnik, B., Valla, P.G., Herman, F., 2016a. Trapped-charge thermochronometry and thermometry: A status review. Chemical Geology 446, 3–17.

King, G.E., Herman, F., Lambert, R., Valla, P.G., Guralnik, B., 2016b. Multi-OSL-thermochronometry of feldspar. Quaternary Geochronology 33, 76–87.

Krbetschek, M.R., Götze, J., Dietrich, A., Trautmann, T., 1997. Spectral information from minerals relevant for luminescence dating. Radiation Measurements 27, 695–748.

Liritzis, I., Stamoulis, K., Papachristodoulou, C., Ioannides, K., 2013. A re-evaluation of radiation dose-rate conversion factors. Mediterranean Archaeology and Archaeometry 13, 1–15.

Mahon, K.I., 1996. The new "york" regression: Application of an improved statistical method to geochemistry. International Geology Review 38, 293–303.

Murray, A.S., Buylaert, J.P., Thomsen, K.J., Jain, M., 2009. The effect of preheating on the IRSL signal from feldspar. Radiation Measurements 44, 554–559.

Omar, G.I., Lutz, T.M., Giegengack, R., 1994. Apatite fission-track evidence for Laramide and post-Laramide uplift and anomalous thermal regime at the Beartooth overthrust, Montana-Wyoming. GSA Bulletin 106, 74–85.

Pagonis, V., Brown, N.D., 2019. On the unchanging shape of thermoluminescence peaks in pre-heated feldspars: Implications for temperature sensing and thermochronometry. Radiation Measurements 124, 19–28.

Pagonis, V., Morthekai, P., Kitis, G., 2014. Kinetic analysis of thermoluminescence glow curves in feldspar: evidence for a continuous distribution of energies. Geochronometria 41, 168–177.

Rhodes, E.J., 2015. Dating sediments using potassium feldspar single-grain IRSL: initial methodological considerations. Quaternary International 362, 14–22.

Sanderson, D.C.W., 1988. Fading of thermoluminescence in feldspars: characteristics and corrections. Nuclear Tracks and Radiation Measurments 14, 155–161.

Schmidt, C., Friedrich, J., Adamiec, G., Cruscinska, A., Fasoli, M., Kreutzer, S., Martini, M., Panzeri, L., Polymeris, G.S., Przegietka, K., Valla, P.G., King, G.E., Sanderson, D.C.W., 2018. How reproducible are kinetic parameter constraints of quartz luminescence? An interlaboratory comparison for the 110 °C TL peak. Radiation Measurements 110, 14–24.

Spencer, J.Q., Sanderson, D.C.W., 1994. Mapping thermal exposure by luminescence thermometry. Radiation Measurements 23, 465–468.

Spencer, J.Q.G., Sanderson, D.C.W., 2012. Decline in firing technology or poorer fuel resources? High-temperature thermoluminscence (HTTL) archaeothermometry of Neolithic ceramics from Pool, Sanday, Orkney. Journal of Archaeological Science 39, 3542–3552.

Tang, S.L., Li, S.H., 2017. Low temperature thermochronology using thermoluminescence signals from K-feldspar. Geochronometria 44, 112–120.

Valla, P.G., Lowick, S.E., Herman, F., Champagnac, J.D., Steer, P., Guralnik, B., 2016. Exploring $IRSL_{50}$ fading variability in bedrock feldspars and implications for OSL thermochronometry. Quaternary Geochronology 36, 55–66.

Wise, D.U., 2000. Laramide structures in basement and cover of the Beartooth uplift near Red Lodge, Montana. AAPG Bulletin 84, 360–375.

Ypma, P., Hochman, M., 1991. Thermoluminescence geothermometry - a case study of the Otway Basin. The Australian Petroleum Exploration Association Journal 35, 312–324.

List of Figures

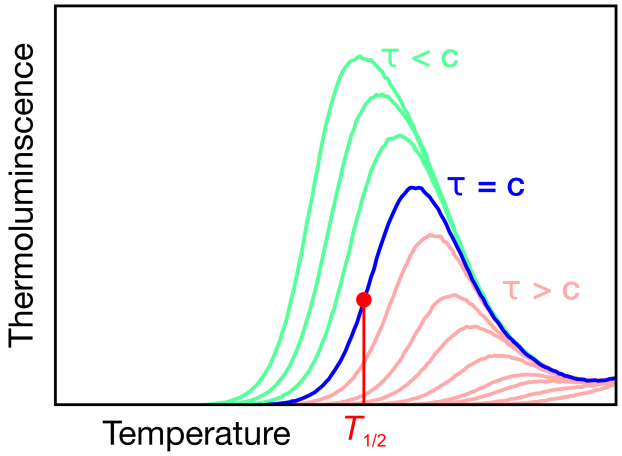

Figure 1: Thermoluminescence curves that would result following preheats of increasing temperature or duration are shown. The stability of the least stable occupied traps giving rise to the blue curve can be described with the $T_{1/2}$ metric (lower of the two measurement temperatures at half-maximum intensity) shown in red. Those least stable traps would have some mean lifetime τ. In green are curves with lesser minimum lifetimes and in pink are curves with greater minimum lifetimes.

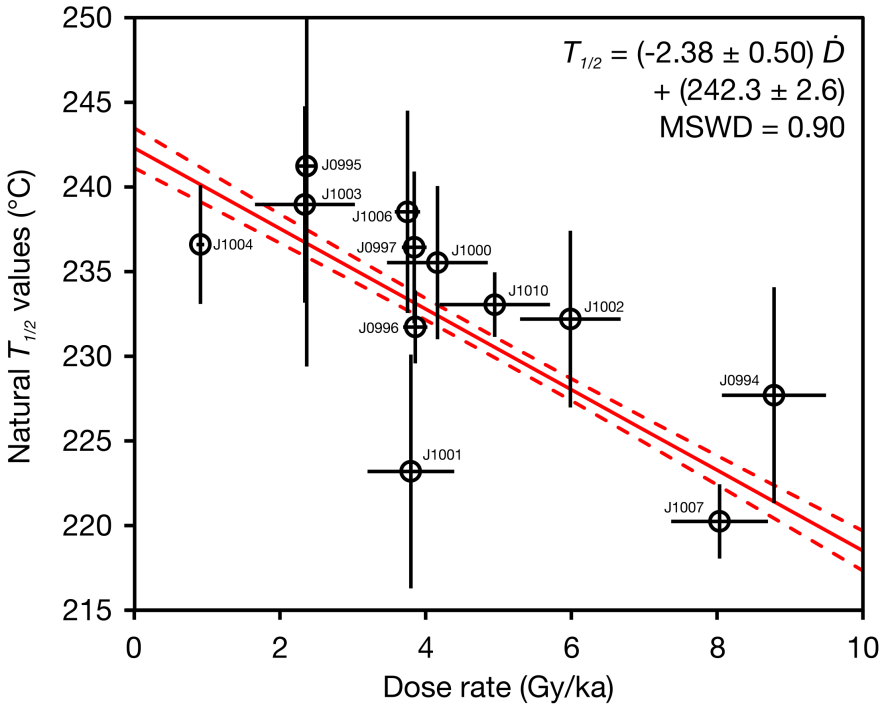

Figure 2: The $T_{1/2}$ values from natural TL curves ($\beta = 5$ °C/s) show a linear dependence upon the geologic dose rate as predicted by theory: at higher dose rates, the $T_{1/2}$ value for the leading edge of TL emissions shifts to lower temperatures. The interpretation is that traps of lower stability can remain occupied due to the high dose rate.

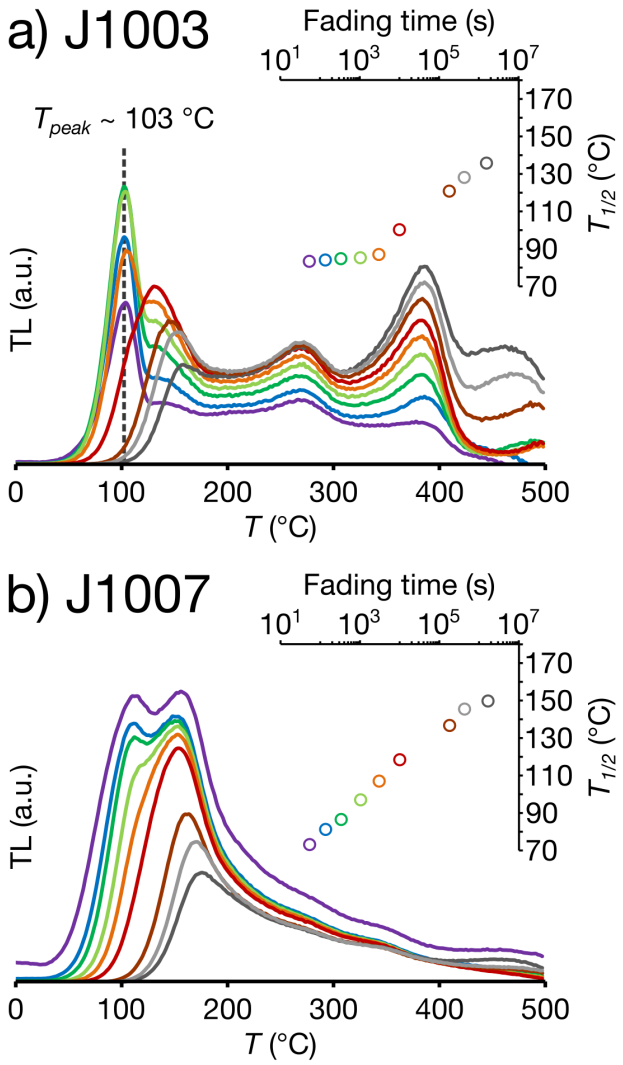

Figure 3: The TL responses after room temperature fading are shown for samples J1003 (a) and J1007 (b). The $T_{1/2}$ values of these curves are plotted as a function of effective fading time within the insets. Notice how the peak centered at 103 °C complicates the behavior of sample J1003.

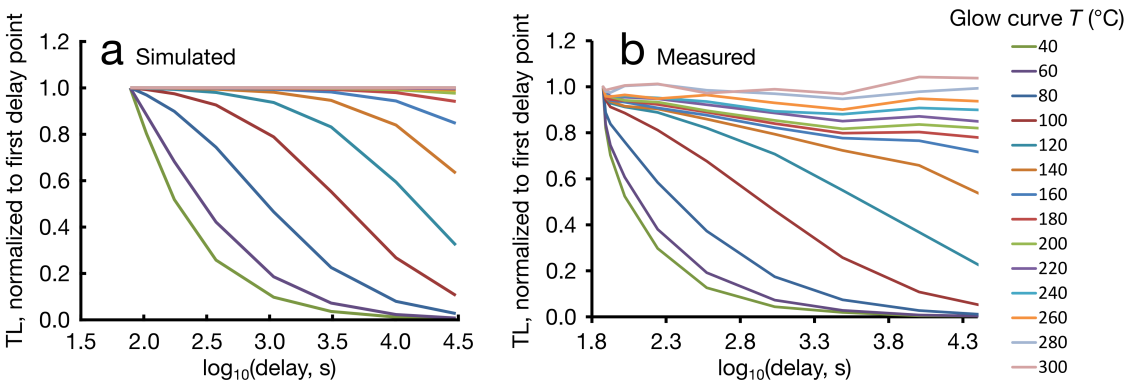

Figure 4: Comparison of simulated (a) and measured (b) TL decay as a function of storage time at room temperature. Different curves represent different glow curve temperatures. The same delay times and glow curve temperatures are shown in each panel.

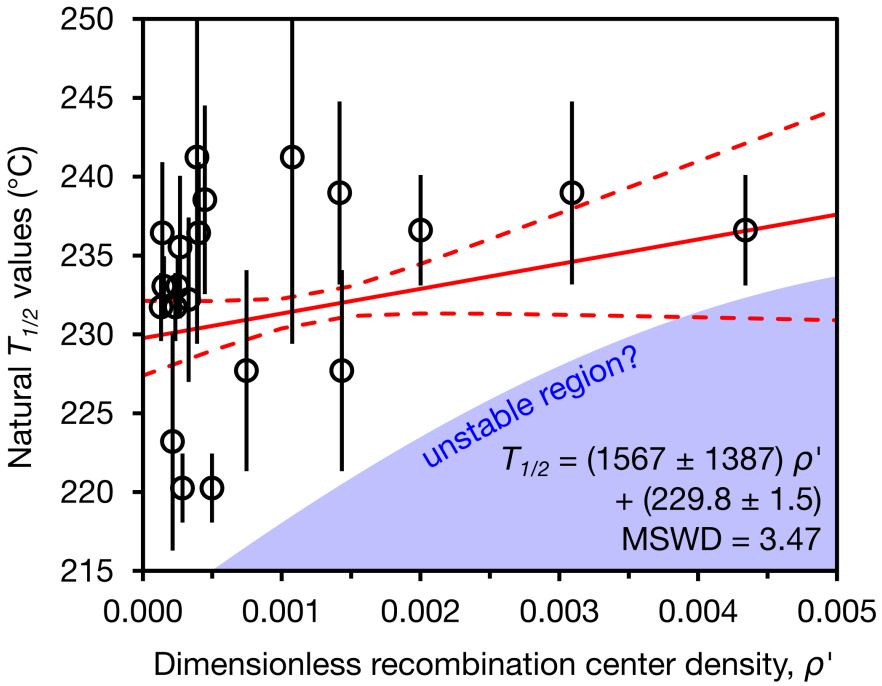

Figure 5: The $T_{1/2}$ values from natural TL curves ($\beta = 5$ °C/s) do not show a significant correlation with ρ' values derived from room-temperature fading measurements. However, note that while a wide range of $T_{1/2}$ values are observed at lower ρ' values, at higher ρ' values (i.e., higher fading rates) natural $T_{1/2}$ values are higher. This is suggested by the blue region which may represent an unstable region wherein fading is too great for charge to accumulate at lower regions of the TL glow curve.